AIAA JOURNAL
Vol. 30, No. 9, September 1992

Accuracy of Critical-Temperature Sensitivity Coefficients Predicted by Multilayered Composite Plate Theories

Ahmed K. Noor* and Scott Burton†
NASA Langley Research Center, Hampton, Virginia 23665

An assessment is made of the accuracy of the critical-temperature sensitivity coefficients of multilayered plates predicted by different modeling approaches, based on two-dimensional shear-deformation theories. The sensitivity coefficients considered measure the sensitivity of the critical temperatures to variations in different lamination and material parameters of the plate. The standard of comparison is taken to be the sensitivity coefficients obtained by the three-dimensional theory of thermoelasticity. Numerical studies are presented showing the effects of variation in the geometric and lamination parameters of the plate on the accuracy of both the sensitivity coefficients and the critical temperatures predicted by the different modeling approaches.

Nomenclature

d_l = material and lamination parameters of the plate
E_L, E_T = elastic moduli in the direction of fibers and normal to it
G_{LT}, G_{TT} = shear moduli in the plane of fibers and the plane normal to it
h = total thickness of the plate
h_k, h_{k-1} = distances from the bottom and top surfaces of the kth layer to the middle plane of the plate (see Fig. 1)
J_β, $\bar{J}$, J_3 = parameters identifying the numbers of displacement and strain components [see Eqs. (19), (20), and (23)]
$[K_0]$ = linear stiffness matrix of the plate [see Eqs. (33)]
$[K_0]_0$, $[K_0]_1$, $[K_0]_2$ = components of the matrix $[K_0]$ [see Eqs. (A.5)]
$[K_1]$, $[K_2]$ = matrices of initial stresses and initial displacements [see Eqs. (33)]
k_1^0, k_2^0, k_1, k_2 = initial and corrected values of the composite shear correction factors
L_1, L_2 = side lengths of the plate
m, n = Fourier harmonics in the x_1 and x_2 directions
NL = total number of layers of the plate
$S_{\beta\gamma}^{(j)}$, $S_{\beta 3}^{(j)}$, $S_{33}^{(j)}$ = stress resultants [see Eqs. (25)]
T_{cr} = critical value of T^0
T^0 = uniform temperature change
$T_{\beta\gamma}^{0(j)}$ = initial (prebuckling) stress resultants [see Eqs. (25)]
t_{ij} ($i, j = 1, 2, 3$) = stress components [see Eqs. (10)]
U_{13}^0, U_{23}^0, $\bar{U}_{13}$, $\bar{U}_{23}$ = transverse shear strain energy densities obtained from the first-order shear deformation theory and the three-dimensional equations, respectively (see Appendix A)
u_β^0, u_β = initial (prebuckling) and total displacements in the x_α coordinate directions [see Eqs. (7)]
v_β, ω = perturbation displacement components in the x_α and x_3 directions, respectively [see Eqs. (7) and (8)]
$v_\beta^{(j)}$, $\omega^{(j)}$ = perturbation displacement expansion parameters [see Eqs. (19) and (20)]
w^0, w = initial (prebuckling) and total transverse displacements [see Eqs. (8)]
$\{X\}_{mn}$ = vector of displacement parameters of the plate associated with the pair of harmonics (m, n); see Eqs. (33)
x_β, x_3 = Cartesian coordinate system
α_0 = normalization factor for the coefficients of thermal expansion
α_L, α_T = coefficients of thermal expansion of the individual layers in the direction of fibers and normal to it, respectively
ϵ = infinitesimal
ϵ_{ij}, ϵ_{ij}^0 ($i, j = 1, 2, 3$) = total and initial strain components [see Eqs. (9)]
$\eta_{\beta\gamma}$, $2\eta_{\beta 3}$, η_{33} = in-plane, transverse shear, and transverse normal strains of the plate [see Eqs. (13–15)]
$\eta_{\beta\gamma}^j$, $2\eta_{\beta 3}^j$, η_{33}^j = strain expansion parameters [see Eqs. (21–23)]
θ = fiber orientation angle
ν_{LT}, ν_{TT} = Poisson's ratios for the material of the individual layers
$\lambda = \alpha_0 T_{cr}$ = critical temperature parameter
ξ_β, ζ = dimensionless coordinates (see Fig. 1)
π = total potential energy
σ_{ij}, σ_{ij}^0 ($i, j = 1, 2, 3$) = total and prebuckling stress components [see Eqs. (10)]
τ_{11}, τ_{22}, τ_{33} = normal stress components associated with adjacent (buckling) configuration
τ_{12}, τ_{13}, τ_{23} = shear stress components associated with adjacent (buckling) configuration
ψ_{ij} ($i, j = 1, 2, 3$) = strain components [see Eqs. (9) and (16)]
$\psi_{\beta\gamma}^{(j)}$ = strain parameters [see Eqs. (24)]
δ, δ^2 = symbols of first and second variations
∂_i = $\partial/\partial x_i$

Subscripts

β, γ, ρ = 1, 2
i, j = 1, 2, 3

Received Aug. 5, 1991; revision received Dec. 16, 1991; accepted for publication Dec. 16, 1991.

*Ferman W. Perry Professor of Aerospace Structures and Applied Mechanics and Director, Center for Computational Structures Technology, University of Virginia. Fellow AIAA.

†Research Scientist, Center for Computational Structures Technology, University of Virginia. Member AIAA.

m, n = (m, n) Fourier harmonics
L = direction of fibers
T = direction transverse to the fibers

Superscripts

$2i, 2i+1$ = symmetric and antisymmetric (in-the-thickness direction) sets of the response quantities
$\hat{}$ = symmetric component of the response quantities in the thickness direction
$\tilde{}$ = antisymmetric component of the response quantities in the thickness direction

Introduction

BECAUSE of the variability of elastic and thermal properties of multilayered composite laminates, an increasing amount of attention has been devoted to the study of the sensitivity of their response to variations in material and lamination parameters. Recent studies on the subject include development of simple analytic expressions for the derivatives of various stiffness and thermal coefficients of composite laminates with respect to each of the material properties and fiber orientation angles of individual layers[1] and study of the sensitivity of the free vibration frequencies, critical temperatures, and postbuckling response of multilayered composite plates to variations in different material and lamination parameters.[2-4] Although the cited studies have contributed to an understanding of the influence of material and lamination parameters on the vibration and buckling of thermally stressed plates, they have not provided any information about the accuracy of the sensitivity coefficients predicted by two-dimensional multilayered plate theories. Several studies have used two-dimensional theories for predicting the thermal buckling response of multilayered plates: classical lamination theory (see, for example, Refs. 5-7); first-order shear deformation theory based on linear displacement variation through-the-thickness of the entire laminate[8-10]; and higher-order shear deformation theories based on nonlinear variations of displacements.[11,12] The present study focuses on the accuracy of the sensitivity coefficients calculated by two-dimensional shear deformation theories. Specifically, our objective is to assess the accuracy of the critical-temperature sensitivity coefficients predicted by different modeling approaches, based on two-dimensional shear deformation theories. The sensitivity coefficients considered measure the sensitivity of the critical temperatures to variations in different lamination and material parameters of the plate. The modeling approaches considered are based on five global approximation shear deformation theories and the two predictor-corrector procedures described in Refs. 13 and 14. The shear deformation theories differ in the thickness variation of the in-plane displacements v_β and the transverse displacement ω, ranging from linear v_α and constant ω (first-order shear deformation theory) to quintic variation of both v_β and ω. The standard of comparison is taken to be the sensitivity coefficients obtained by the three-dimensional theory of thermoelasticity.

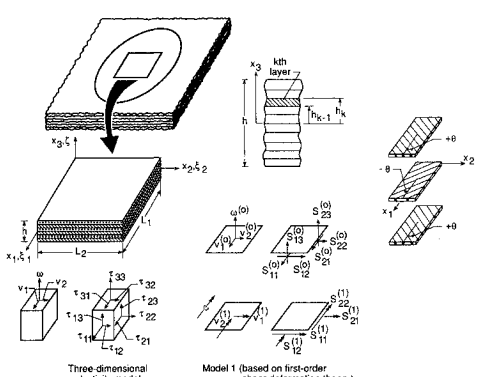

Fig. 1 Laminated anisotropic plates and sign convention for displacements, stresses, and stress resultants.

The composite plates considered herein consist of a number of perfectly bonded layers which have antisymmetric lamination with respect to the middle plane. The individual layers are assumed to be homogeneous and anisotropic. At each point of the plate a plane of thermoelastic symmetry exists parallel to the middle plane. The temperature change is assumed to be uniform (independent of x_1, x_2, and x_3), and the material properties are assumed to be independent of temperature. All response quantities are assumed to be periodic in the surface coordinates. The sign convention for the different displacement components is shown in Fig. 1.

The particular anisotropic laminates, temperature change, prebuckling state, and periodic response selected in the present study allowed exact three-dimensional and two-dimensional solutions to be obtained. Extensive numerical results are presented showing the effects of variation in the lamination and geometric parameters of the plates on the accuracy of the sensitivity coefficients obtained by the different modeling approaches.

Mathematical Formulation

Figure 1 shows the geometric characteristics of the plate segment considered as follows: L_1 and L_2 are the side lengths in the x_1 and x_2 directions, and h is the total thickness of the plate. The dimensionless coordinates ξ_1, ξ_2, and ζ are introduced, where

$$\xi_\beta = x_\beta / L_\beta \tag{1}$$

$$\zeta = x_3 / h \tag{2}$$

In Eq. (1), $\beta = 1, 2$ and β is not summed.

In the present study the three-dimensional thermoelastic model is used as the standard for assessing the accuracy of the two-dimensional models. The fundamental equations of the three-dimensional thermoelasticity used in the present study are given in Ref. 15.

In succeeding subsections the three-dimensional relations governing the prebuckling state, buckling mode, and stability criterion are listed. The kinematic relations used in developing the two-dimensional shear deformation theories are given, along with the associated strain and stress resultant parameters. A procedure is outlined for obtaining exact solutions for the two-dimensional model equations governing the thermal response and its sensitivity coefficients.

Prebuckling Displacements and Stresses

The prebuckling displacements and stresses generated by the uniform temperature rise T_0 are assumed to be independent of x_1 and x_2 and can be written in the following form:

$$u_\beta^0 = 0 \tag{3}$$

$$w^0 = w^0(T^0) \tag{4}$$

$$\sigma_{\beta\gamma}^0 = \sigma_{\beta\gamma}^0(T^0) \tag{5}$$

$$\sigma_{i3}^0 = 0 \tag{6}$$

where the superscript 0 refers to the prebuckling state, w^0 is a linear function of x_3, $\beta, \gamma = 1, 2$, and $i = 1$-3.

The prebuckling displacements and stresses [Eqs. (3-6)] satisfy all of the fundamental equations of the three-dimensional nonlinear theory of elasticity within each layer, the equilibrium and continuity conditions at the interfaces between layers, and the stress-free boundary conditions at the top and bottom surfaces of the plate.[15] All of the prebuckling stresses

Table 1 Modeling approaches used in the numerical studies

Model no.	Description	Through-the-thickness displacement assumptions	Constraint conditions on stresses	Total no. of displacement parameters	No. of strain parameters (and stress resultants)
1, 1A	First-order shear-deformation theory[a]	Linear v_α and constant ω ($J_\beta = 1$, $J_3 = 0$)	$\tau_{33} = 0$	5	8
2	First-order theory with transverse normal stresses and strains included	Linear v_α and ω ($J_\beta = J_3 = 1$)	None	6	11
3	Lo-Christensen-Wu type theory	Cubic v_α, quadratic ω ($J_\beta = 3$, $J_3 = 2$)	None	11	20
4	Higher-order shear deformation theory	Quintic v_α and ω ($J_\beta = J_3 = 5$)	None	18	35
5	Simplified higher-order theory	Cubic v_α, constant ω ($J_\beta = 1$, $J_3 = 0$)	$\tau_{33} = 0$ throughout the $\tau_{\alpha 3}$ at top and bottom surfaces	5	13
6A, 6B, 6C	Predictor-corrector approach (see Refs. 14, 18, and 19)	Predictor phase: Linear v_α, constant ω Corrector phase:—[b]	Predictor phase: $\tau_{33} = 0$ Corrector phase: None	5	8

[a]In model 1, $k_1^0 = k_2^0 = 1$, and in model 1A, $k_1^0 = k_2^0 = 5/6$.
[b]In models 6A and 6B the corrector phase is based on adjusting the transverse shear stiffnesses, and in model 6C it is based on correcting the thickness distributions of v_α and ω. Model 6B accounts for $\partial k_\beta / \partial d_t$, whereas model 6A neglects these terms (see Appendix A). In models 6A, 6B, and 6C the initial $k_1^0 = k_2^0$ are selected to be 1.
For the definition of J_β and J_3, see Eqs. (19) and (20).

$\sigma^0_{\beta\gamma}$ are linear in T^0, and the prebuckling displacement w^0 is a nonlinear function of T^0. The prebuckling stresses and displacements are obtained from the stress-displacement relations and the continuity conditions at layer interfaces.[15]

Buckling Mode

The buckling mode is assumed to correspond to an adjacent configuration with the following values of displacements:

$$u_\beta = u^0_\beta + \epsilon v_\beta \tag{7}$$

$$w = w^0 + \epsilon\omega \tag{8}$$

where ϵ is an infinitesimal; v_β and ω are the perturbation displacement components. The resulting strains and stresses have the following form:

$$\epsilon_{ij} = \epsilon^0_{ij} + \epsilon\eta_{ij} + \epsilon^2\psi_{ij} \tag{9}$$

$$\sigma_{ij} = \sigma^0_{ij} + \epsilon\tau_{ij} + \epsilon^2 t_{ij} \tag{10}$$

where

$$\epsilon^0_{\beta\gamma} = \epsilon^0_{\beta 3} = 0 \tag{11}$$

$$\epsilon^0_{33} = \partial_3 w^0 + \tfrac{1}{2}(\partial_3 w^0)^2 \tag{12}$$

$$\eta_{\beta\gamma} = \tfrac{1}{2}(\partial_\beta v_\gamma + \partial_\gamma v_\beta) \tag{13}$$

$$\eta_{\beta 3} = \tfrac{1}{2}[\partial_3 v_\beta + (1 + \partial_3 w^0)\partial_\beta\omega] \tag{14}$$

$$\eta_{33} = (1 + \partial_3 w^0)\partial_3\omega \tag{15}$$

$$\psi_{\beta\gamma} = \tfrac{1}{2}(\partial_\beta v_\rho\, \partial_\gamma v_\rho + \partial_\beta\omega\, \partial_\gamma\omega) \tag{16}$$

$$\partial_\beta \equiv \frac{\partial}{\partial x_\beta}, \qquad \partial_3 = \frac{\partial}{\partial x_3}; \qquad i, j = 1\text{–}3;\ \beta, \gamma, \rho = 1, 2$$

and the repeated index ρ in Eqs. (16) denotes summation over the range 1, 2. Note that the expressions for $\psi_{\beta 3}$, ψ_{33} in terms of the displacement gradients are not given since they are not needed in the present analysis. The same applies to the stress components t_{ij}. The displacement components v_β and ω, the strain components η_{ij}, and stress components τ_{ij} will henceforth be referred to as the perturbation displacements, strains, and stresses, respectively.

Stability Criterion

The Trefftz stability criterion states that the transition from stable to unstable equilibrium occurs when the second variation of the total potential energy of the plate is stationary, i.e.,

$$\delta(\delta^2\pi) = 0 \tag{17}$$

where

$$\delta^2\pi = \int_V (\tau_{\beta\gamma}\eta_{\beta\gamma} + 2\tau_{\beta 3}\eta_{\beta 3} + \tau_{33}\eta_{33} + 2\sigma^0_{\beta\gamma}\psi_{\beta\gamma})\, dV \tag{18}$$

and where π is the total potential energy of the plate, δ and δ^2 are the symbols of first and second variations, and V is the volume of the plate. The repeated index γ in Eq. (18) denotes summation over the range 1, 2.

Displacement and Stress Resultant Expansions for the Two-Dimensional Models

The two-dimensional shear-deformation theories considered herein are based on global displacement expansions in the thickness coordinate x_3:

$$v_\beta = \sum_{j=0}^{J_\beta} v^{(j)}_\beta \times (x_3)^j \tag{19}$$

$$\omega = \sum_{j=0}^{J_3} \omega^{(j)} \times (x_3)^j \tag{20}$$

where the number of terms in the v_β and ω expansions are $J_\beta + 1$ and $J_3 + 1$, respectively, and $v^{(j)}_a$, $\omega^{(j)}$ are functions of x_1 and x_2 only.

The strain expansions consistent with Eqs. (19) and (20) are

$$\eta_{\beta\gamma} = \sum_{j=0}^{J_\beta} \eta^{(j)}_{\beta\gamma} \times (x_3)^j \tag{21}$$

$$\eta_{33} = \sum_{j=0}^{J_3 - 1} \eta^{(j)}_{33} \times (x_3)^j \tag{22}$$

$$\eta_{\beta 3} = \sum_{j=0}^{\bar{J}} \eta^{(j)}_{\beta 3} \times (x_3)^j \tag{23}$$

and

$$\psi_{\beta\gamma} = \sum_{j=0}^{2\bar{J}} \psi^{(j)}_{\beta\gamma} \times (x_3)^j \tag{24}$$

where $\bar{J} = \max(J_\beta - 1 \text{ and } J_3)$, and the strain parameters $\eta^{(j)}_{\beta\gamma}$, $\eta^{(j)}_{33}$, $\eta^{(j)}_{\beta 3}$, and $\psi^{(j)}_{\beta\gamma}$ are functions of x_1 and x_2 only.

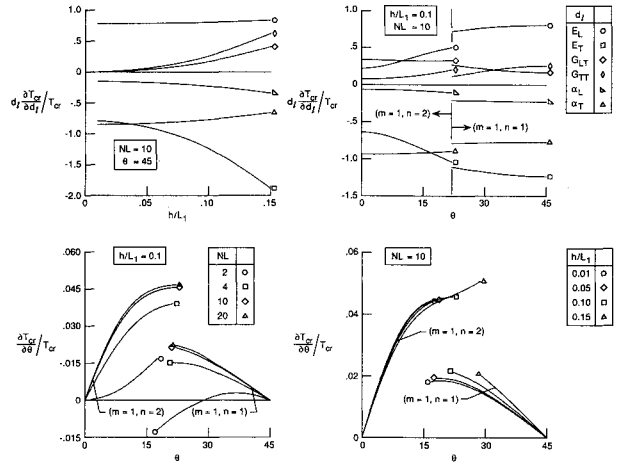

Fig. 2 Effect of lamination and geometric parameters on the critical-temperature sensitivity coefficients obtained by the three-dimensional thermoelasticity model.

The perturbation and initial stress resultants, associated with the strain parameters $\eta^{(j)}_{\beta\gamma}$, $\eta^{(j)}_{33}$, $\eta^{(j)}_{\beta 3}$, and $\psi^{(j)}_{\beta\gamma}$, are defined as follows[14]:

$$\begin{Bmatrix} S_{\beta\gamma} \\ S_{\beta 3} \\ S_{33} \\ T^0_{\beta\gamma} \end{Bmatrix}^{(j)} = \sum_{k=1}^{NL} \int_{h_{k-1}}^{h_k} \begin{Bmatrix} \tau_{\beta\gamma} \\ \tau_{\beta 3} \\ \tau_{33} \\ \sigma^0_{\beta\gamma} \end{Bmatrix} \times (x_3)^j \, dx_3 \tag{25}$$

where $j = 0, 1, \ldots$; h_{k-1} and h_k are the distances from the bottom and top surfaces of the kth layer to the middle plane of the plate; NL is the total number of layers; and piecewise integration is used because of the discontinuity of the stresses at layer interfaces. The number of stress resultants is equal to the number of strain parameters in the theory [which is a function of the number of displacement parameters in the expansion, i.e., the values of J_β and J_3 in Eqs. (19) and (20)].

First-Order Shear Deformation Model

Note that the first-order shear deformation plate model corresponds to $J_\beta = 1$ and $J_3 = 0$. The five displacement parameters of this model are $v^{(0)}_\beta$, $\omega^{(0)}$, and $v^{(1)}_\beta$. The associated eight strain parameters and stress resultants are $\eta^{(0)}_{\beta\gamma}$, $\eta^{(1)}_{\beta\gamma}$, $\eta^{(0)}_{\beta 3}$; $S^{(0)}_{\beta\gamma}$, $S^{(1)}_{\beta\gamma}$, and $S^{(0)}_{\beta 3}$ ($\beta, \gamma = 1, 2$) (see Fig. 1).

Symmetric and Antisymmetric Components of Response Quantities and Their Trigonometric Expansions

To obtain analytic solutions, each of the plate variables is decomposed into symmetric and antisymmetric components in the thickness coordinate and is expressed as the sum of products of trigonometric functions in the Cartesian surface coordinates. The trigonometric functions are chosen so that the displacements, strains, and stress resultants are periodic in x_1 and x_2 with periods $2L_1$ and $2L_2$.

The following expressions are used for the perturbation displacement components and stress resultants.[14]

Symmetric response quantities:

$$\begin{Bmatrix} v_1 \\ v_2 \\ \omega \end{Bmatrix}^{(2i)} = \sum_{m=0} \sum_{n=0} \begin{Bmatrix} v^{(2i)}_{1mn} \sin m\pi\xi_1 \cos n\pi\xi_2 \\ v^{(2i)}_{2mn} \cos m\pi\xi_1 \sin n\pi\xi_2 \\ \omega^{(2i)}_{mn} \sin m\pi\xi_1 \sin n\pi\xi_2 \end{Bmatrix} \tag{26}$$

$$\begin{Bmatrix} S_{11} \\ S_{22} \\ S_{33} \end{Bmatrix}^{(2i)} = \sum_{m=0} \sum_{n=0} \begin{Bmatrix} S_{11_{mn}} \\ S_{22_{mn}} \\ S_{33_{mn}} \end{Bmatrix}^{(2i)} \cos m\pi\xi_1 \cos n\pi\xi_2 \tag{27}$$

$$\begin{Bmatrix} S_{23} \\ S_{13} \\ S_{12} \end{Bmatrix}^{(2i)} = \sum_{m=0} \sum_{n=0} \begin{Bmatrix} S^{(2i)}_{23_{mn}} \sin m\pi\xi_1 \cos n\pi\xi_2 \\ S^{(2i)}_{13_{mn}} \cos m\pi\xi_1 \sin n\pi\xi_2 \\ S^{(2i)}_{12_{mn}} \sin m\pi\xi_1 \sin n\pi\xi_2 \end{Bmatrix} \tag{28}$$

Antisymmetric response quantities:

$$\begin{Bmatrix} v_1 \\ v_2 \\ \omega \end{Bmatrix}^{(2i+1)} = \sum_{m=0} \sum_{n=0} \begin{Bmatrix} v^{(2i+1)}_{1mn} \cos m\pi\xi_1 \sin n\pi\xi_2 \\ v^{(2i+1)}_{2mn} \sin m\pi\xi_1 \cos n\pi\xi_2 \\ \omega^{(2i+1)}_{mn} \cos m\pi\xi_1 \cos n\pi\xi_2 \end{Bmatrix} \tag{29}$$

$$\begin{Bmatrix} S_{11} \\ S_{22} \\ S_{33} \end{Bmatrix}^{(2i+1)} = \sum_{m=0} \sum_{n=0} \begin{Bmatrix} S_{11_{mn}} \\ S_{22_{mn}} \\ S_{33_{mn}} \end{Bmatrix}^{(2i+1)} \sin m\pi\xi_1 \sin n\pi\xi_2 \tag{30}$$

$$\begin{Bmatrix} S_{23} \\ S_{13} \\ S_{12} \end{Bmatrix}^{(2i+1)} = \sum_{m=0} \sum_{n=0} \begin{Bmatrix} S^{(2i+1)}_{23_{mn}} \cos m\pi\xi_1 \sin n\pi\xi_2 \\ S^{(2i+1)}_{13_{mn}} \sin m\pi\xi_1 \cos n\pi\xi_2 \\ S^{(2i+1)}_{12_{mn}} \cos m\pi\xi_1 \cos n\pi\xi_2 \end{Bmatrix} \tag{31}$$

The displacement expansions [Eqs. (26) and (29)] are periodic in x_1 and x_2 with periods $2L_1$ and $2L_2$ and satisfy the following conditions on the middle plane ($x_3 = 0$):

$$\begin{aligned} &\text{at} \quad x_1 = 0, L_1, \qquad u_1 = w = 0 \\ &\text{at} \quad x_2 = 0, L_2, \qquad u_2 = w = 0 \end{aligned} \tag{32}$$

The expansions of the strain parameters are similar to those of the corresponding stress resultants.

Governing Equations for the Two-Dimensional Models

The governing displacement equations are obtained by using Eqs. (19–25) in conjunction with the stability criterion [Eq. (17)] and replacing the perturbation stress resultants by their expressions in terms of the displacement parameters,[14] and then replacing the displacement parameters by their trigono-

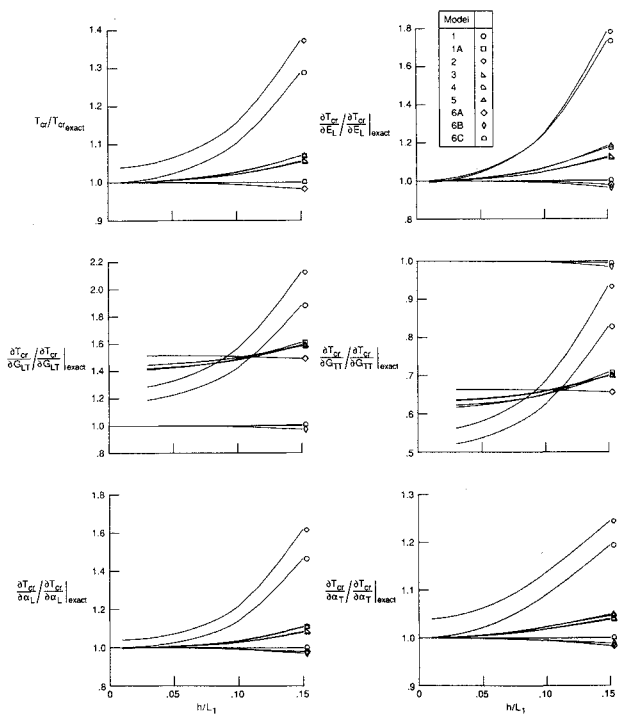

Fig. 3 Effect of thickness ratio, h/L_1, on the accuracy of the critical temperatures and the sensitivity coefficients obtained by the different models listed in Table 1. Ten-layered antisymmetrically laminated angle-ply composite plates, $\theta = 45$ deg, $m = n = 1$.

metric expansions [Eqs. (26) and (29)]. For antisymmetrically laminated plates, the governing equations uncouple in harmonics. For each pair of harmonics, m and n in the x_1 and x_2 directions, the governing displacement equations can be written in the following compact form:

$$[[K_0]_{mn} + \lambda[K_1]_{mn} + [K_2(\lambda)]_{mn}]\{X\}_{mn} = 0 \tag{33}$$

where $\{X\}_{mn}$ is the vector of displacement parameters $v_{\beta mn}^{(j)}$, $\omega_{mn}^{(j)}$; $\lambda = \alpha_0 T_{cr}$ is the critical temperature parameter; α_0 is a normalization factor for the coefficients of thermal expansion; $[K_0]_{mn}$ is the linear stiffness matrix of the plate; $[K_1]_{mn}$ is the matrix of initial stresses, which is independent of the temperature parameter; and $[K_2]_{mn}$ is the matrix containing the initial displacement w^0 (a nonlinear function of λ).

Sensitivity of the Thermal Buckling Response to Variations in Lamination and Material Parameters

The expressions for the sensitivity coefficients of the critical temperature parameter λ, with respect to the lamination and material parameters, d_l, of a composite plate are given by

$$\frac{\partial\lambda}{\partial d_l} = \{X\}^t\left(\frac{\partial[K_0]}{\partial d_l} + \lambda\frac{\partial[K_1]}{\partial d_l} + \frac{\partial[K_2]}{\partial d_l}\right)\{X\}$$
$$/\{X\}^t \times \left([K_1] + \left[\frac{\partial K_2}{\partial\lambda}\right]\right)\{X\} \tag{34}$$

Analytical expressions are given in Ref. 1 for the laminate stiffnesses and thermal coefficients and their derivatives with respect to each of the material properties and fiber orientation angles. The evaluation of $\partial[K_0]/\partial d_l$ and $\partial[K_2]/\partial d_l$ in the predictor-corrector procedures is described in Appendix A.

Numerical Studies

To study the effect of variations in the material characteristics and fiber orientation of individual layers on the accuracy of the sensitivity coefficients obtained by different modeling approaches, a large number of thermal buckling problems of multilayered composite plates have been solved. For each problem the critical temperature and the sensitivity coefficients obtained by nine different models were compared with those obtained by the three-dimensional theory of thermoelasticity. The method of obtaining the three-dimensional solutions is outlined in Refs. 15–17. The modeling approaches are listed in Table 1. The first six are based on two-dimensional shear deformation theories and differ in the thickness variation of v_α and ω as follows: first-order shear deformation theory based on linear variation of v_α and constant ω. Two different values of the composite shear correction factors are used, namely, 1 and 5/6 (models 1 and 1A); first-order theory based on linear variation of v_α and ω (model 2); higher-order theory based on cubic variation of v_α and quadratic variation of ω (model 3); higher-order theory based on quintic variation of v_α and ω (model 4); and a simplified higher-order theory based on cubic variation of v_α and constant ω with the conditions of zero transverse shear stresses imposed at the outer surfaces of the plate to reduce the number of generalized displacement parameters (model 5). The remaining three models (models 6A, 6B, and 6C) are based on predictor-corrector procedures. The three models use first-order shear deformation theory in the predictor phase, but differ in the elements of the computational model being adjusted in the corrector phase. The corrected quantities in the models are then used in conjunction with the three-dimensional equations to obtain better estimates for the critical temperature and the sensitivity coefficients. Models 6A and 6B calculate a posteriori estimates of the composite correction factors k_α and use them to adjust the transverse shear stiffnesses of the plate. Model 6B accounts for $\partial k_\alpha/\partial d_l$, whereas model 6A neglects these terms (see Appendix A). Model 6C calculates a posteriori the functional dependence of the displacement components on the thickness coordinate and uses these as coordinate functions in the Rayleigh-Ritz approximation of the three-dimensional equations.

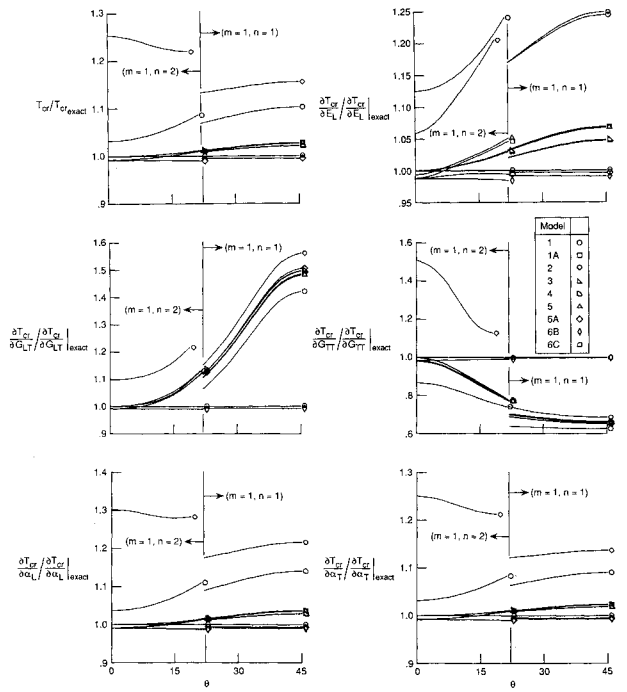

Fig. 4 Effect of fiber orientation angle on the critical temperatures and the sensitivity coefficients obtained by the different models listed in Table 1. Ten-layered antisymmetrically laminated angle-ply composite plates, $h/L_1 = 0.1$

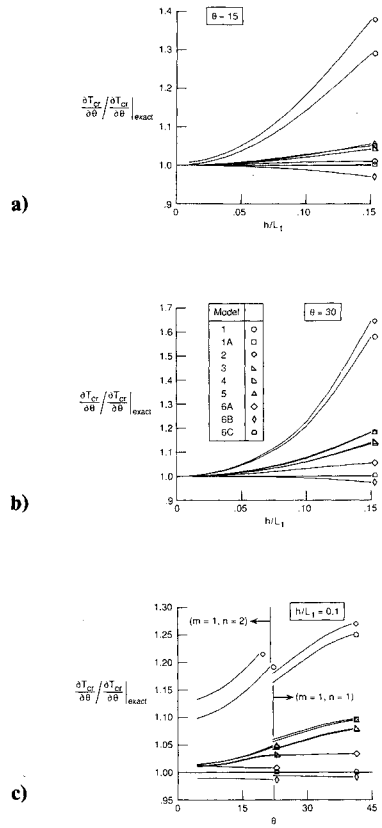

Fig. 5 Effect of h/L_1 and θ on the accuracy of $\partial T_{cr}/\partial\theta$ obtained by the different models listed in Table 1. Ten-layered antisymmetrically laminated angle-ply composite plates. a) $m = 1$, $n = 2$; b) $m = n = 1$; c) $m = 1$, $n = 1$ and $m = 1$, $n = 2$.

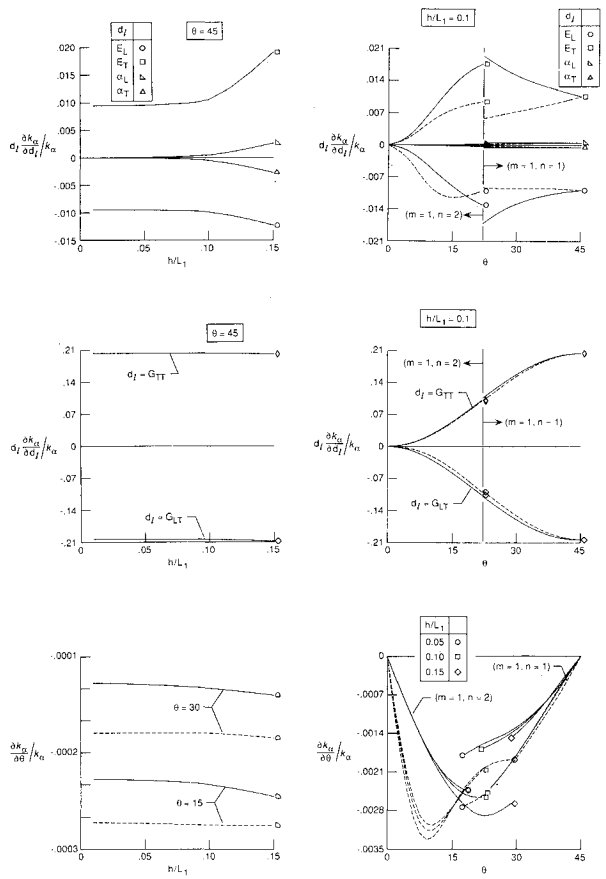

Fig. 6 Effect of lamination and geometric parameters on the sensitivity coefficients of the shear correction factors. Ten-layered antisymmetrically laminated angle-ply composite plates. In the left three figures $m = n = 1$, except for the case $\theta = 15$ deg $m = 1$, $n = 2$. Solid lines and dashed lines are used for k_1 and k_2, respectively.

The composite plates considered in the present study are square angle-ply laminates having antisymmetric lamination with respect to the middle plane with fiber orientation alternating between $+\theta$ and $-\theta$ and with $L_1 = L_2 = 1.0$. The thermal buckling responses are assumed to be periodic in x_1 and x_2 with periods $2L_1$ and $2L_2$.

The material properties of the individual layers are taken to be those typical of high-modulus fibrous composites, namely,

$$E_L/E_T = 15, \qquad G_{LT}/E_T = 0.5, \qquad G_{TT}/E_T = 0.3356$$

$$\nu_{LT} = 0.3, \qquad \nu_{TT} = 0.49$$

$$\alpha_L/\alpha_0 = 0.015, \qquad \alpha_T/\alpha_0 = 1.0$$

where the subscript L refers to the direction of fibers, and the subscript T refers to the transverse direction; ν_{LT} is the major Poisson's ratio; and α_0 is a normalization factor for the coefficients of thermal expansion. The temperature is assumed to be uniform. Only the lowest critical temperatures and the associated sensitivity coefficients are considered.

Three parameters are varied: the fiber orientation angle of the individual layers θ, the number of layers NL, and the thickness ratio of the plate h/L_1. The thickness ratio was varied between 0.01 and 0.15, the number of layers was varied between 2 and 20, and θ was varied between 0 and 45 deg. Typical results are shown in Figs. 2-6 and are discussed subsequently.

The effects of variation of the three parameters h/L_1, θ, and NL on the sensitivity coefficients $\partial T_{cr}/\partial d_l$ and $\partial T_{cr}/\partial\theta$, obtained by the three-dimensional theory of thermoelasticity, are shown in Fig. 2, where d_l refers to any of the material properties E_L, E_T, G_{LT}, G_{TT}, α_L, or α_T. The sensitivity coefficients are normalized by dividing each by the corresponding critical temperature T_{cr} and for $\partial T_{cr}/\partial d_l$ by multiplying each derivative by d_l. For thin plates ($h/L_1 < 0.05$), the critical temperature is more sensitive to variations in E_L, E_T, α_T, and α_L than to variations in other material properties (viz., G_{LT} and G_{TT}). As h/L_1 increases to 0.15, T_{cr} becomes sensitive to variations in the shear moduli G_{LT} and G_{TT} as well. The sensitivity coefficients $\partial T_{cr}/\partial E_T$, $\partial T_{cr}/\partial G_{TT}$, and $\partial T_{cr}/\partial\alpha_T$ increase with the increase of both h/L_1 and θ; $\partial T_{cr}/\partial G_{LT}$ increases with the increase in increasing h/L, but decreases with increasing θ. The sensitivity coefficient $\partial T_{cr}/\partial d_L$ decreases with the increase in both h/L_1 and θ; and $\partial T_{cr}/\partial E_L$ is insensitive to variations in h/L_1 and increases with increasing θ. The sensitivity coefficient $\partial T_{cr}/\partial\theta$ increase with increasing NL, and for 30 deg $< \theta <$ 45 deg these coefficients increase with increasing h/L_1. Note that the discontinuities in the plots for the sensitivity coefficients vs θ is due to the changes in the buckling mode and are located at the values of θ for which these mode changes occur.

An indication of the accuracy of the minimum critical temperature and the associated sensitivity coefficients obtained by the models listed in Table 1 is given in Figs. 3-5. In Fig. 3 the ratios $T_{cr}/T_{cr_{exact}}$ and $(\partial T_{cr}/\partial d_l)/(\partial T_{cr}/\partial d_l)|_{exact}$ are plotted vs h/L_1, and in Fig. 4 they are plotted vs θ. In Fig. 5 plots are shown of the ratios $(\partial T_{cr}/\partial\theta)/(\partial T_{cr}/\partial\theta)|_{exact}$ vs h/L_1 for $\theta = 15$ and 30 deg as well as the same ratios vs θ for $h/L_1 = 0.1$. The discontinuities in the plots shown in Figs. 4 and 5 are due to modal changes. An examination of Figs. 3-5 reveals the following:

1) In general, the sensitivity coefficients $\partial T_{cr}/\partial d_l$ predicted by the different models are less accurate than the corresponding critical temperatures, T_{cr}. This is particularly true for medium thick plates with $h/L_1 \geq 0.10$. Exceptions to this are the sensitivity coefficients predicted by the predictor-corrector models 6B and 6C, which are nearly as accurate as the critical temperature predicted by the same models.

2) For $d_l = E_L$, α_L, and α_T the variation of $(\partial T_{cr}/\partial d_l)/(\partial T_{cr}/\partial d_l)|_{exact}$ with h/L_1 is qualitatively similar to that of $T_{cr}/T_{cr_{exact}}$ (see Figs. 3 and 5). The same is true for the variation of $\partial T_{cr}/\partial\alpha_L$ and $\partial T_{cr}/\partial\alpha_T$ with θ (see Fig. 4). Specifically,

a) The predictions of Model 2 are the least accurate among the models considered.

b) The sensitivity coefficients predicted by model 1A are as accurate as those predicted by model 5 and are considerably more accurate than those predicted by model 1.

c) The accuracy of $\partial T_{cr}/\partial d_l$ obtained by model 3 is comparable to that of model 4 and is higher than the accuracy of $\partial T_{cr}/\partial d_l$ obtained by other models, based on two-dimensional theories.

d) The sensitivity coefficients obtained by the predictor-corrector procedures, models 6B and 6C, are very accurate for all of the ranges of the parameters considered.

3) For $\theta \geq 15$ deg the sensitivity coefficients $\partial T_{cr}/\partial G_{LT}$ and $\partial T_{cr}/\partial G_{TT}$ obtained by models 3 and 4 are considerably less accurate than the other sensitivity coefficients obtained by the same models.

4) The use of model 6A in which variations of the composite correction factors with d_l, $\partial k_\beta/\partial d_l$ ($\beta = 1, 2$) are neglected results in reasonably accurate sensitivity coefficients with respect to the fiber orientation angle θ, as well as with respect to all the material parameters other than the shear moduli G_{LT} and G_{TT} (see Figs. 3 and 4). The accurate prediction of $\partial T_{cr}/\partial G_{LT}$ and $\partial T_{cr}/\partial G_{TT}$ requires the incorporation of $\partial k_\beta/\partial d_l$ in the expressions of the sensitivity coefficients (see Appendix A). As can be seen, this is because $\partial k_\beta/\partial\theta$ are very small, and for $\theta \geq 15$ the values of $\partial k_\beta/\partial G_{LT}$ and $\partial k_\beta/\partial G_{TT}$ are one order of magnitude higher than the other derivatives of k_β (see Fig. 6). Note that $\partial k_\beta/\partial G_{LT}$ is of opposite sign to $\partial k_\beta/\partial G_{TT}$. Both derivatives increase with increasing θ and are relatively insensitive to variations in h/L_1.

The aforementioned observations point to the fact that the accurate prediction of the sensitivity coefficients requires the use of more accurate computational models than the response predictions. The predictor-corrector procedures provide inexpensive and effective modeling approaches for evaluating both the various response quantities, as well as their sensitivity coefficients.

Concluding Remarks

An assessment is made of the accuracy of the critical-temperature sensitivity coefficients obtained by nine different models. Six of the models are based on two-dimensional shear deformation theories. The remaining three are based on predictor-corrector procedures. The standard of comparison is taken to be the analytic sensitivity coefficients obtained by the three-dimensional theory of thermoelasticity.

The six two-dimensional models differ in the thickness variation of the displacements v_β and ω as follows: first-order shear deformation theory based on linear variation of v_β and constant ω; two different values of the composite shear correction factors are used with these models (namely, 1 and 5/6); first-order theory based on linear variation of both v_β and ω; higher-order theory based on cubic variation of v_β and quadratic variation of ω; higher-order theory based on quintic variation of v_β and ω; and a simplified higher-order theory based on cubic variation of v_β and constant ω with the conditions of zero transverse shear stresses imposed at the outer surfaces of the plate to reduce the number of generalized displacement parameters.

The three models based on predictor-corrector procedures use first-order shear deformation theory in the predictor phase, but differ in the elements of the computational model being adjusted in the corrector phase. The first procedure calculates a posteriori estimates of the composite correction factors and uses them to adjust the transverse shear stiffnesses of the plate. The second model, in addition to calculating a posteriori the composite shear correction factors, takes into account the derivatives of these correction factors with respect to each of the material and lamination parameters. The third procedure calculates a posteriori the functional dependence of the displacement components on the thickness coordinate. The corrected quantities are then used in conjunction with the three-dimensional equations to obtain better estimates for the different sensitivity coefficients.

Extensive numerical results are presented for multilayered antisymmetrically laminated plates showing the effects of variation of the geometric and lamination parameters on the accuracy of the critical-temperature sensitivity coefficients obtained by different models. On the basis of the numerical results the following conclusions are justified:

1) The sensitivity coefficients predicted by the different models are, in general, less accurate than the corresponding critical temperatures. This is particularly true for medium thick plates with $h/L_1 \geq 0.10$.

2) The accuracy of both the sensitivity coefficients and the critical temperatures predicted by the first-order shear deformation theory is strongly dependent on the values of the composite correction factors. The use of the value of 5/6 for composite correction factors results in comparable accuracy to that obtained by the simplified higher-order theory.

3) Although the critical temperatures predicted by the higher-order shear deformation theories are fairly accurate for a wide range of geometric and lamination parameters, the corresponding sensitivity coefficients are not as accurate. This is particularly true for the coefficients with respect to G_{LT} and G_{TT}.

4) The predictor-corrector procedures appear to be very effective procedures for the accurate determination of the sensitivity coefficients, as well as for the critical temperature and detailed thermal buckling response characteristics of multilayered plates. The accuracy of the sensitivity coefficients obtained in the first (predictor) phase for laminates with thickness to wavelength (of the deformation) ratio of the order of 0.1 may be unacceptable. However, the corrector phase improves the predictions substantially and results in highly accurate sensitivity coefficients. This is true for the procedure that incorporates the coefficients of the composite correction factors, as well as for the procedure based on calculating a posteriori the functional dependence of the displacements on thickness coordinates. The latter procedure works well even for thick laminates with thickness-to-wavelength ratio >0.15.

Appendix A: Evaluation of the Composite Correction Factors and $\partial[K_0]/\partial d_l$ in the Predictor-Corrector Procedures

In models 6A and 6B, a posteriori estimates of the composite shear correction factors are calculated by equating the integrals of the transverse shear strain energy densities (energy per unit area of the middle plane) obtained from the first-order shear deformation theory to those obtained by integrating, through the thickness, the corresponding energy per unit volume, obtained from the three-dimensional equations.[18,19] The formulas for evaluating k_1 and k_2 can be written in the following form:

$$k_1 \bar{U}_{13} = (k_1^0)^2 U_{13}^0 \tag{A1}$$

$$k_2 \bar{U}_{23} = (k_1^0)^2 U_{23}^0 \tag{A2}$$

where U_{13}^0, U_{23}^0 and $\bar{U}_{13}$, $\bar{U}_{23}$ are the transverse shear strain energy densities (energy per unit area of the middle plane) obtained from the first-order shear deformation theory and the three-dimensional equations, respectively; k_1^0, k_2^0 and k_1, k_2 are the initial and corrected estimates of the composite shear factors. The expressions for $U_{\beta 3}^0$, $\bar{U}_{\beta 3}$ ($\beta = 1, 2$) in terms of the stress resultants, stresses and strain components are given by

$$\begin{Bmatrix} k_1^0 & U_{13}^0 \\ k_2^0 & U_{23}^0 \end{Bmatrix} = \frac{1}{2}\begin{Bmatrix} S_{13}^{(0)} \times 2\eta_{13}^{(0)} \\ S_{23}^{(0)} \times 2\eta_{23}^{(0)} \end{Bmatrix} \tag{A3}$$

$$\begin{Bmatrix} \bar{U}_{13} \\ \bar{U}_{23} \end{Bmatrix} = \sum_{k=1}^{NL} \int_{h_{k-1}}^{h_k} \frac{1}{2}\begin{Bmatrix} \tau_{13} \times (2\eta_{13}) \\ \tau_{23} \times (2\eta_{23}) \end{Bmatrix} dx_3 \tag{A4}$$

For antisymmetrically laminated plates the two matrices $[K_0]$ and $[K_2]$ in the governing equations of the plate [Eqs. (33)] can be written as the sum of three matrices as follows:

$$[K_0] = [K_0]_0 + k_1[K_0]_1 + k_2[K_0]_2 \tag{A5}$$

and

$$[K_2] = [K_2]_0 + k_1[K_2]_1 + k_2[K_2]_2 \tag{A6}$$

where $[K_0]_0$ and $[K_2]_0$ contain the extensional and bending stiffnesses of the plate; $[K_0]_1$, $[K_0]_2$, $[K_2]_1$, and $[K_2]_2$ contain the transverse shear stiffnesses of the plate.

The derivatives of $[K_0]$ with respect to d_l can therefore be expressed as follows:

$$\frac{\partial[K_0]}{\partial d_l} = \frac{\partial[K_0]_0}{\partial d_l} + k_1\frac{\partial[K_0]_1}{\partial d_l} + k_2\frac{\partial K_0]_2}{\partial d_l} + \frac{\partial k_1}{\partial d_l}[K_0]_1 + \frac{\partial k_2}{\partial d_l}[K_0]_2 \tag{A7}$$

with a similar expression for $\partial[K_2]/\partial d_l$.

The derivatives of the composite shear correction factors with respect to d_l are obtained by differentiating Eqs. (A1) and (A2). The resulting expressions are

$$\frac{\partial k_1}{\partial d_l} = \left[(k_1^0)^2\frac{\partial U_{13}^0}{\partial d_l} - k_1\frac{\partial \bar{U}_{13}}{\partial d_l}\right] \Big/ \bar{U}_{13} \tag{A8}$$

$$\frac{\partial k_2}{\partial d_l} = \left[(k_2^0)^2 \frac{\partial U_{23}^0}{\partial d_l} - k_2 \frac{\partial \bar{U}_{23}}{\partial d_l} \right] \Big/ \bar{U}_{23} \tag{A9}$$

Note that in model 6A the derivatives $\partial k_1/\partial d_l$ and $\partial k_2/\partial d_l$ are neglected.

Acknowledgment

The present research is partially supported by NASA Cooperative Agreement NCCW-0011 and by an Air Force Office of Scientific Research Grant AFOSR-90-0369. The authors appreciate the encouragement of Samuel L. Venneri of NASA Headquarters and Spencer Wu of AFOSR and acknowledge useful discussions with James H. Starnes, Jr., of NASA Langley.

References

[1]Noor, A. K., and Tenek, L. H., "Stiffness and Thermoelastic Coefficients for Composite Laminates," *Journal of Composite Structures*, Vol. 21, No. 1, 1992, pp. 57–66.

[2]Noor, A. K., and Peters, J. M., "Thermomechanical Buckling of Multilayered Composite Plates," *Journal of Engineering Mechanics*, Vol. 118, No. 2, 1992, pp. 351–366.

[3]Noor, A. K., and Burton, W. S., "Three-Dimensional Solutions for the Free Vibrations and Buckling of Thermally Stressed Multilayered Angle-Ply Composite Plates," *Journal of Applied Mechanics* (to be published).

[4]Noor, A. K., and Peters, J. M., "Thermal Postbuckling of Thin-Walled Composite Stiffeners," *Computing Systems in Engineering*, Vol. 2, No. 1, 1991, pp. 1–16.

[5]Whitney, J. M., and Ashton, J. E., "Effect of Environment on the Elastic Response of Layered Composite Plates," *AIAA Journal*, Vol. 9, No. 9, 1971, pp. 1708–1713.

[6]Tauchert, T. R., and Huang, N. N., "Thermal Buckling of Symmetric Angle-Ply Laminated Plates," *Composite Structures 4, Proceedings of the Fourth International Conference on Composite Structures*, edited by I. N. Marshall, Elsevier, Amsterdam, 1987, pp. 1.424–1.435.

[7]Thangaratnam, K. R., Palaninathan, R., and Ramachandran, J., "Thermal Buckling of Composite Laminated Plates," *Computers and Structures*, Vol. 32, No. 5, 1989, pp. 1117–1124.

[8]Stavsky, Y., "Thermoelastic Stability of Laminated Orthotropic Circular Plates," *Acta Mechanica*, Vol. 22, No. 1/2, 1975, pp. 31–51.

[9]Chen, L. W., Brunelle, E. J., and Chen, L. Y., "Thermal Buckling of Initially Stressed Thick Plates," *Journal of Mechanical Design*, Vol. 104, July 1982, pp. 557–564.

[10]Tauchert, T. R., "Thermal Buckling of Thick Antisymmetric Angle-Ply Laminates," *Journal of Thermal Stresses*, Vol. 10, No. 2, 1987, pp. 113–124.

[11]Sun, L. X., and Hsu, T. R., "Thermal Buckling of Laminated Composite Plates with Transverse Shear Deformation," *Computers and Structures*, Vol. 36, No. 5, 1990, pp. 883–889.

[12]Chang, J. S., "FEM Analysis of Buckling and Thermal Buckling of Antisymmetric Angle-Ply Laminates According to Transverse Shear and Normal Deformable High-Order Displacement Theory," *Computers and Structures*, Vol. 37, No. 6, 1990, pp. 925–946.

[13]Noor, A. K., Burton, W. S., and Peters, J. M., "Predictor-Corrector Procedure for Stress and Free Vibration Analyses of Multilayered Composite Plates and Shells," *Computer Methods in Applied Mechanics and Engineering*, Vol. 82, Nos. 1–3, 1990, pp. 341–364.

[14]Noor, A. K., and Burton, W. S., "Predictor-Corrector Procedures for Thermal Buckling of Multilayered Composite Plates," *Computers and Structures*, Vol. 40, No. 5, 1991, pp. 1071–1084.

[15]Noor, A. K., and Burton, W. S., "Three-Dimensional Solutions for Thermal Buckling of Multilayered Anisotropic Plates," *Journal of Engineering Mechanics*, Vol. 118, No. 4, pp. 683–701.

[16]Srinivas, S., and Rao, A. K., "Bending, Vibration and Buckling of Simply Supported Thick Orthotropic Rectangular Plates and Laminates," *International Journal of Solids and Structures*, Vol. 6, No. 11, 1970, pp. 1463–1481.

[17]Srinivas, S., "A Refined Analysis of Composite Laminates," *Journal of Sound and Vibration*, Vol. 30, No. 4, 1973, pp. 495–507.

[18]Noor, A. K., and Burton, W. S., "Stress and Free Vibration Analyses of Multilayered Composite Plates," *Journal of Composite Structures*, Vol. 11, No. 3, 1989, pp. 183–204.

[19]Noor, A. K., and Peters, J. M., "A Posteriori Estimates for Shear Correction Factors in Multilayered Composite Cylinders," *Journal of Engineering Mechanics*, Vol. 115, No. 6, June 1989, pp. 1225–1244.